

Atmosphere-ionosphere conductivity enhancements during a hard solar energetic particle event

M. Kokorowski,¹ A. Seppälä,^{2,3} J. G. Sample,⁴ R. H. Holzworth,⁵ M. P. McCarthy,⁵ E. A. Bering,⁶ and E. Turunen^{7,8}

Received 20 November 2011; revised 27 March 2012; accepted 27 March 2012; published 17 May 2012.

[1] On 20 January 2005, a solar energetic particle (SEP) event caused the largest recorded solar proton ground level event since 1956. Serendipitously, a balloon-borne experiment intended to measure effects of relativistic electron precipitation was aloft over Antarctica (~ 32 km; near 70° S, 345° E geographic) throughout the duration of the SEP event, including the fast (~ 6 min) onset. The balloon instrumentation included dc electric field and scalar electrical conductivity sensors. The observed conductivity increased by nearly a factor of 20 above ambient with the SEP event onset and returned to within a factor of two above normal levels within 17 h. Results from a newly developed, globally applicable atmosphere-ionosphere conductivity model based on the Sodankylä Ion and Neutral Chemistry (SIC) model suggest that proton-induced ionization was directly responsible for the observed conductivity increase at the balloon. Model input for this event included estimates of ionization from energetic particle precipitation and rigidity cutoffs. Altitudes between 20 and 150 km were considered during model runs. The results show a maximum conductivity increase near 60 km of more than 600-fold directly after SEP event onset. Relatively small conductivity enhancements (two- to fivefold) are suggested to have occurred above 70 km as a result of SEP ionization, while almost no enhancement is thought to have occurred above 95 km. These results quantify the real effect that an SEP-event can have on atmosphere-ionosphere electrical conductivity on a large, nearly global scale and provide a detailed comparison to one of the few direct stratospheric conductivity observations made during an SEP event.

Citation: Kokorowski, M., A. Seppälä, J. G. Sample, R. H. Holzworth, M. P. McCarthy, E. A. Bering, and E. Turunen (2012), Atmosphere-ionosphere conductivity enhancements during a hard solar energetic particle event, *J. Geophys. Res.*, *117*, A05319, doi:10.1029/2011JA017363.

1. Introduction

[2] Atmospheric electrical conductivity values can vary spatially as a function of altitude over 14 orders of magnitude between the ground and the ionospheric dynamo layer near 120 km. In the middle atmosphere (between 40 and

80 km) the conductivity can vary with time up to six orders of magnitude at a given altitude between extremely quiescent periods and intense proton precipitation events (see Figure 1) [Hale, 1984]. The predominant ionization source in the lower atmosphere is cosmic ray radiation, which is modulated by the solar cycle [e.g., Tinsley and Zhou, 2006]. In the middle and upper atmosphere, solar ultraviolet becomes increasingly important. Generally speaking, conductivity increases exponentially with altitude as neutral density decreases. In the polar regions, episodes of intense solar proton precipitation can contribute to the ionization, causing significant deviations from the nominal background [e.g., Reid, 1986]. Figure 1, adapted from Hale [1984], provides example conductivity profiles for nominal day, nominal night and during a solar energetic particle (SEP) event.

[3] SEP event precipitation into the atmosphere is a subauroral to polar phenomena. In the case study presented here, conductivity model results are compared with stratospheric balloon data before and during an extremely hard SEP event on 20 January 2005. This SEP event was the hardest solar proton ground level event (GLE) on record since 1956 [Mewaldt et al., 2005]. The MINIature Spectrometer (MINIS) Balloon Campaign had one payload aloft

¹Jet Propulsion Laboratory, California Institute of Technology, Pasadena, California, USA.

²British Antarctic Survey/Natural Environment Research Council, Cambridge, UK.

³Now at Earth Observation, Finnish Meteorological Institute, Helsinki, Finland.

⁴Space Sciences Laboratory, University of California Berkeley, Berkeley, California, USA.

⁵Department of Earth and Space Science, University of Washington, Seattle, Washington, USA.

⁶Physics Department, University of Houston, Houston, Texas, USA.

⁷Sodankylä Geophysical Observatory, Sodankylä, Finland.

⁸Now at EISCAT Scientific Association, Kiruna, Sweden.

Corresponding author: M. Kokorowski, Jet Propulsion Laboratory, California Institute of Technology, Pasadena, CA 91109, USA. (Michael.Kokorowski@jpl.nasa.gov)

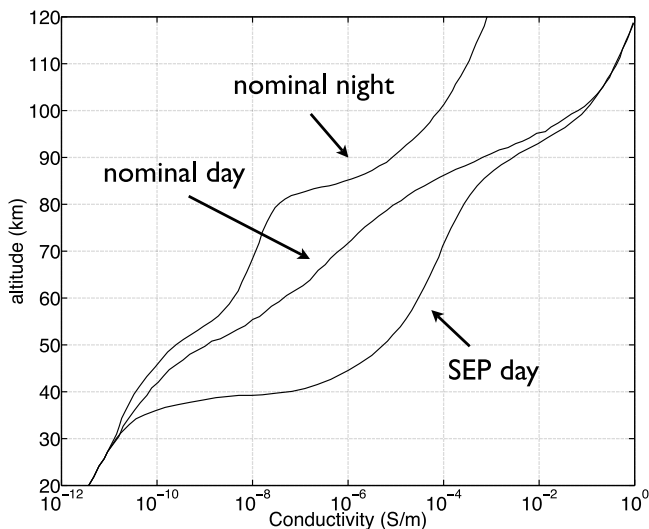


Figure 1. A sample of nominal day, night and SEP conductivity profiles. The SEP conductivity is based on a rocket flight from Churchill, Manitoba, Canada during an SEP event on November 3, 1969. (Adapted from Hale [1984], Figure 3).

over Antarctica for the duration of the SEP event, which lasted about one day. The MINIS balloon payload had a dc electric field instrument, which made conductivity measurements using the relaxation technique [e.g., Byrne *et al.*, 1988] every 10 min. Directly following the SEP event onset, the MINIS instrumentation measured a nearly 20-fold local conductivity increase [Kokorowski *et al.*, 2006]. This marks only the second time that stratospheric conductivity has been measured by in situ balloon instrumentation during an SEP event [cf. Holzworth *et al.*, 1987].

[4] The conductivity model presented here uses ion density output from the Sodankylä Ion and Neutral Chemistry (SIC) model. Thus, we refer to the model as the SIC-based conductivity model. The SIC model has the capability to produce ion density profiles between 20 and 150 km altitude at any location on the globe for 36 positive and 28 negative ion species, including multiple hydrated species [Verronen, 2006]. Additionally, ionization from particle precipitation can easily be included as an altitude-dependent source term. In recent years, the SIC model has begun to be used outside of atmospheric chemistry, specifically within the field of ionospheric and space physics. The SIC model has been used to study various phenomena during energetic particle precipitation events, including whistler-induced electron precipitation [Rodger *et al.*, 2007], VLF radio wave propagation [Clilverd *et al.*, 2006] and ozone population dynamics during an SEP event [Seppälä *et al.*, 2004; 2006; 2008].

[5] The effects of SEP precipitation are not limited to conductivity enhancements. SEP events have been observed to cause polar cap absorption (PCA), during which high-frequency radio waves that normally propagate through the ionosphere become more heavily absorbed [Bailey, 1964]. Reid [1961] shows that, using an approximation of the Appleton-Hartree formalism, absorption at a given atmospheric location is directly related to the electron number

density. Therefore, SEP-induced ionization enhancements can cause increased radio absorption. This absorption can, in turn, cause space to ground/aircraft communication disruption, particularly in the 1–100 MHz range. Example disruptions can affect GPS signals and airplane avionics [Jones *et al.*, 2005]. SEP events have been shown to effect a variety of neutral atmospheric chemistry as well. SEP-induced HO_x and NO_x enhancements are shown to be connected to ozone depletion during several SEP events for a number of events between 2000 and 2003 [Jackman *et al.*, 2005a], for the extremely solar active period of October–November 2003 [Jackman *et al.*, 2005b; Verronen *et al.*, 2005], and the January 2005 events [Seppälä *et al.*, 2006, 2008]. In fact, both of the papers by Seppälä *et al.* [2006, 2008] use the SIC model to study the effects of the hard SEP events in a very similar fashion as presented here. Those efforts focus mainly on important atmospheric chemistry interactions associated with ozone. The work described here focuses on the effects of the 20 January 2005 SEP event from an atmospheric electricity point of view.

[6] The remainder of this paper is structured as follows. There is a brief discussion of the atmosphere/ionosphere conductivity theory and a description of the SIC-based conductivity model and its constituent building blocks. This is followed by a description of the MINIS balloon conductivity instrumentation and the measurements made on 20 January 2005. A comparison of the model and data showing good agreement within the error of the measurements is shown. Finally, the conductivity model is applied to the entire altitude range for a full day on 20 January 2005 before and during a hard SEP event.

2. Atmosphere-Ionosphere Conductivity Model

[7] The SIC-based conductivity model is a tool that is built upon several standard model tools that estimate neutral density, magnetic field, and ion density. In this section the tensor expression used as the basis of this conductivity model is presented. Then, the standard model tools used are briefly mentioned. The SIC model is described in slightly more detail before a full discussion of the proton-induced ionization modeling method is presented. Last, the SIC-based conductivity model output without any external forcing is presented for comparison with nominal values and a separate ionosphere-only conductivity model.

2.1. Conductivity in the Atmosphere-Ionosphere

[8] The medium we are considering is the plasma in the collisional atmosphere and the lower ionosphere. Here, collisional atmosphere is defined as the region of the atmosphere where there are no free electrons (generally below ~70 km). The altitude range considered is between 20 and 150 km. These limits were chosen because they are the limits of the SIC model. In the strictest sense, the collisional atmosphere and lower ionosphere are not traditional plasmas because there are many more neutrals than charge carriers.

[9] The movement of charge through a medium is governed by Ohm's law, which connects the current density (\vec{j}) to the electric field (\vec{E}) through the conductivity of the medium ($\vec{\sigma}$).

$$\vec{j} = \vec{\sigma} \vec{E} \quad (1)$$

Table 1. Variable Descriptions for Equations (2)–(5)

Symbol	Description
σ_P	Pedersen conductivity term
σ_H	Hall conductivity term
σ_0	Parallel (to \vec{B}) conductivity term
n_s	Neutral number density
q_s	Charge of carrier
m_s	Charge carrier mass
ν_{sn}	Charge carrier–neutral collision frequency
s	Charge carrier species
Ω_s	Cyclotron frequency of charge carrier

In an atmospheric electricity application with the presence of the Earth's magnetic field, both the current density and electric field are vectors, while conductivity is a tensor. Conductivity in the atmosphere-ionosphere is intimately tied to charge carrier-neutral collision frequency (ν) and cyclotron frequency ($\Omega = qB/m$). Due to gyration effects, in the presence of a magnetic field, conductivity is represented by a tensor, not a scalar. Assuming that the magnetic field is in the \hat{z} direction (which is approximately true in polar regions), the conductivity becomes:

$$\vec{\sigma} = \begin{bmatrix} \sigma_P & \sigma_H & 0 \\ -\sigma_H & \sigma_P & 0 \\ 0 & 0 & \sigma_0 \end{bmatrix} \quad (2)$$

where,

$$\sigma_P = \sum_s \frac{n_s q_s^2}{m_s} \left(\frac{\nu_{sn}}{\nu_{sn}^2 + \Omega_s^2} \right); \quad (3)$$

$$\sigma_H = \sum_s \frac{n_s q_s^2}{m_s} \left(\frac{\Omega_s}{\nu_{sn}^2 + \Omega_s^2} \right); \quad (4)$$

$$\sigma_0 = \sum_s \frac{n_s q_s^2}{m_s \nu_{sn}}. \quad (5)$$

A description of the notation used in equations (2)–(5) is given in Table 1. Complete derivations for this tensor conductivity can be found in multiple sources, including *Parks* [1991], *Holzworth* [1995], and *Kokorowski* [2008]. The nonzero terms along the diagonal in equation (2) allow for current flow in the direction of the electric field, while the Hall term allows for current flow perpendicular to both electric (\vec{E}) and magnetic (\vec{B}) fields. The expressions in equations (3)–(5) are the values calculated in the conductivity model being presented.

2.2. Standard Model Tools

[10] A Mass Spectrometer Incoherent Scatter (MSIS) model (specifically the Naval Research Laboratory's NRLMSISE-00) model was used for neutral atmosphere composition, density and temperature. A complete description of the NRLMSISE-00, along with various error estimates can be found in *Picone et al.* [2002]. The best estimate for errors in neutral density below 90 km is 5% whereas above 90 km errors are estimate to be as high as 20%. (These error values are from *Hedin* [1991] and specifically reference the MSISE-90 model, which does not differ significantly from the NRLMSISE-90 model for neutral densities below 150 km.) Magnetic field values were taken from the International Geomagnetic Reference Field (IGRF) [*Maus et al.*, 2005]. Errors in the IGRF magnetic field are believe to be on the order of 10 nT [*Lowes*, 2010]. For comparison

to the SIC model in the ionosphere above 120 km, the International Reference Ionosphere (IRI) model is used to provide charged particle composition, density and temperature. A complete description of the IRI model is given in a NASA technical memorandum [*Bilitza*, 1990]. The estimated mean error for IRI electron densities between 60 km and 120 km is a factor of 2.6 [*Friedrich and Torkar*, 2001].

[11] The following empirical formula derived from EIC-SAT radar measurements and described by *Kirkwood et al.* [1988] is used as an expression for collision frequency.

$$\begin{aligned} \nu_{in} &= 4.305 \times 10^{-16} (nN_2 + 0.98nO_2 + 0.57nO)s^{-1} \\ \nu_{en} &= 1.5 \times 10^{-17} (nT_e)s^{-1} \end{aligned} \quad (6)$$

Here nN_2 , nO_2 , nO and n are the number densities (m^{-3}) of molecular nitrogen, molecular oxygen, atomic oxygen and the total neutral number density, respectively. The electron temperature is given by T_e (K). The electron temperature is assumed to be equal to the neutral temperature as given by the NRLMSISE-00 model below 120 km and is taken from the IRI model above 120 km.

[12] Figure 2 shows collision frequency and cyclotron frequency for electrons and some dominant ions between 20 km and 150 km. Electron-neutral collision frequency is equal to the electron cyclotron frequency near 70 km. For ions, the collision and cyclotron frequencies are equal near 130 km. The ionospheric dynamo layer is therefore centered between these altitudes. The example in Figure 2 is for a particular time and location (20 January 2005 06:00 UT, 70°S, 345°E geographic) and uses the NRLMSISE-00 and IGRF models to calculate neutral number density, temperature and magnetic field strength. Figures with similar features can be produced for any geographic location and time.

2.3. Sodankylä Ion and Neutral Chemistry Model

[13] Originally, the SIC model was developed to help describe quiet time D region by keeping track of concentrations of multiple ion species (24 positive and 11 negative) [*Turunen et al.*, 1996]. After several revisions, the SIC model now includes 79 different ion and neutral species (36 positives, 28 negatives and 15 neutrals) over an altitude range of 20–150 km. A complete description of the SIC model similar to the version used in this analysis is in the doctoral dissertation of *Verronen* [2006]. Here, SIC version 6.8.1 was used. In order to calculate the concentration of each species, a time-dependent continuity equation of the following form is solved.

$$\frac{\partial n_s}{\partial t} = P_s - L_s n_s - \nabla \cdot (n_s \bar{v}_s) \quad (7)$$

Here, n_s is the number density, P_s is the local production rate, L_s is the local loss rate and \bar{v}_s is the average velocity for a given species s . The last term on the right hand side, $\nabla \cdot (n_s \bar{v}_s)$, is atmospheric vertical transport (e.g., an upward wind). Although equation (7) is a straightforward definition for a given species' number density, one significant challenge in the implementation of the SIC model comes from the large number of species and the complex chemistry involved. Detailed flow diagrams of that representative chemistry can be found in *Verronen* [2006, Figures 4.3 and 4.4].

[14] The SIC model uses daily average 1 AU photon flux rates determined by the SOLAR2000 model (now the Solar

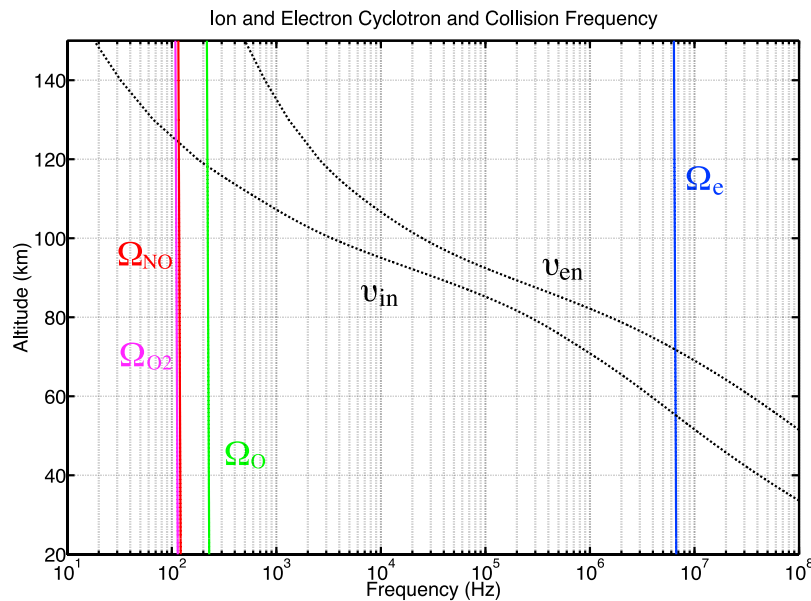


Figure 2. Cyclotron and collision frequencies for electrons and abundant ions. The collision frequencies were calculated using equation (6). The NRLMSISE-00 and IGRF models were used for neutral number densities, temperature and magnetic field values. This model location and time used for this figure are 70°S, 345°E geographic, 06:00 UT on 20 January 2005.

Irradiance Platform) [Tobiska *et al.*, 2000]. The SIC model also includes ionization of N₂ and O₂ by galactic cosmic rays (GCR). The GCR ionization source is parameterized for solar minimum and maximum as according to Heaps [1978].

2.4. SEP Proton-Induced Ionization

[15] The SIC model has the capability to include any ionization source term as an input. In this effort, SEP proton-induced ionization was included. Energetic proton flux from the geosynchronous GOES spacecraft in integral channels between >1 MeV and >100 MeV is used for the SIC proton input. It is assumed that all of the energetic particles measured at geosynchronous will precipitate into the polar cap. The GOES integral proton flux is converted into a differential flux between 600 keV and 2000 MeV using the exponential rigidity spectrum described by Freier and Webber [1963].

$$J = J_0 e^{-P/r_0} \quad (8)$$

Here, J is the integral proton flux and P is the proton rigidity (momentum per unit charge). Over the course of an individual SEP event, Freier and Webber [1963] determined that the flux spectrum was not constant, but the exponential nature of the flux spectrum held true. At a given time, the GOES-measured energetic integral proton spectrum is transformed into a differential spectrum by assuming the relation in equation (8) holds for each pair of integral energy bins. Using the method described above, discontinuities appear when the assumed integral spectrum does not fully characterize the measured spectrum. Figure 3 gives examples of integral and differential spectra two hours after SEP event onset on 20 January 2005. Regardless of what method is used to transform an integral into a differential spectrum,

assumptions must be made that are inherently undetermined by measurements.

[16] After calculating a differential proton flux spectrum, the incident protons are propagated through a model atmosphere using a range-energy relation for protons in air [Bethe and Ashkin, 1953].

$$R(E) = aE^b \quad (9)$$

Here, R is the range, E is the kinetic energy of the proton and a and b are experimentally determined parameters. The amount of energy deposited at a given altitude, $\frac{dE}{dz}$, is calculated based on procedures originally used by Reid [1961] and again by Rees [1989]. The energy deposited can be divided by the average energy lost by an incident proton per ionization ($\Delta\varepsilon = 35eV$ [Rees, 1989]) to get the number of ion-electron pairs created by a single proton at a given altitude. The total proton-induced ionization rate (Q) is calculated by multiplying number of ionizations from a single proton by the differential proton flux, $F(E)$, and integrated over energy and angle.

$$Q(z) = \frac{1}{\Delta\varepsilon} \int \int \int \left(\frac{dE}{dz} \right) F(E) \sin\theta d\theta d\phi dE \quad (10)$$

With equation (10), a solar energetic proton spectrum, like those from GOES, can be used to calculate an ionization rate profile. This SEP-induced ionization rate is used as an ion production term in equation (7). SIC-calculated ion densities are currently estimated to be accurate to within a few tens of percent (*personal communication*, P. Verronen). The SIC-calculated ionization levels have been studied many times during SEP events have been tested experimentally using incoherent scatter radar [Verronen *et al.*, 2002], riometers

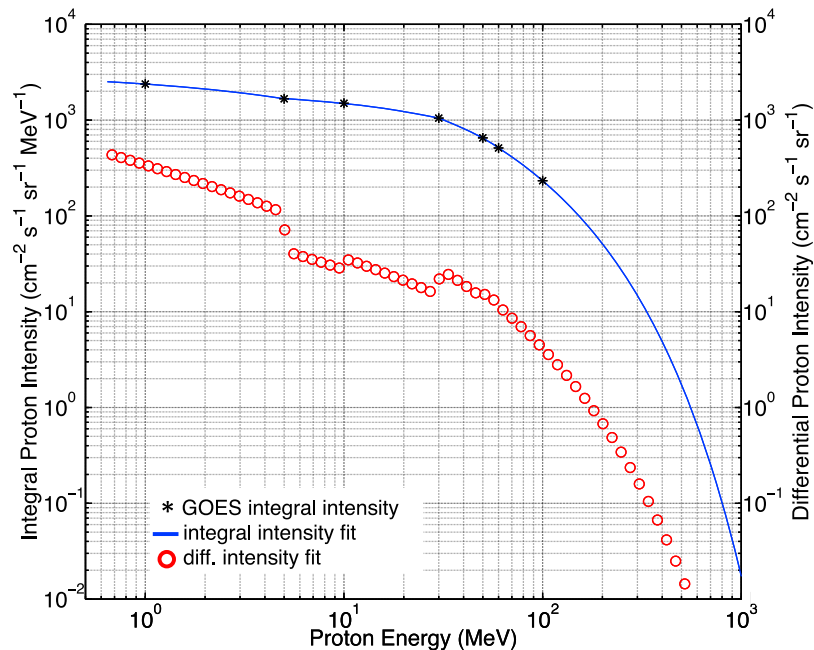


Figure 3. GOES 11 integral and differential proton intensity at 09:00 UT 20 January 2005. The black stars correspond to the GOES 11 integral measurements. The solid blue line is the piecewise fit to the observations. The red circles are the calculated differential proton intensity values. The estimated errors of the proton intensity data are 15%.

[Rodger *et al.*, 2006; Clilverd *et al.*, 2007], and subionospheric VLF propagation [Clilverd *et al.*, 2005].

2.5. Example of SIC-Based Conductivity Model Output

[17] Using the output of each of the models described above, equations (3)–(5) can be solved directly to give an altitude profile of conductivity at a particular location and time. Figure 4 provides two examples of SIC-based conductivity profiles. Also plotted are sets of IRI-based conductivity above 120 km for comparison (where IRI-based conductivity simply uses the charge carrier densities predicted by the IRI model, not SIC). The examples in Figure 4 are specific to 70°S, 345°E geographic at 00:00 UT and 12:00 UT on 20 January 2005, the same day as the large SEP event examined in this case study. Note that no energetic proton precipitation is included in any conductivity calculations shown in Figure 4. The parallel, Pedersen and Hall conductivity profiles are given by black, red and blue lines, respectively. After a visual comparison of the SIC-based parallel conductivity profiles and the compilation in Figure 1, it is clear that the SIC-based model is in reasonable agreement with previous expectations. The parallel term monotonically increases with altitude as the neutral density decreases. Without including any energetic particle ionization, the nominal day and night from Figure 1 roughly agree with the SIC-based parallel conductivity estimates at noon and midnight. With latitude and seasonal differences (and therefore solar irradiance differences) direct one-to-one agreement between the profiles in Figure 1 and Figure 4 would not be expected.

[18] A closer comparison of the IRI-based profiles and the SIC-based profiles again shows good, albeit variable, agreement. Figure 4a shows one of the worst agreements at 00:00 UT which corresponds to local sunrise/sunset, while

Figure 4b shows one of the best in the daytime. In Figures 4a and 4b, the IRI and SIC-based Pedersen and Hall conductivities have a maximum at concurrent altitudes, between 110 km and 130 km. This is what we expect because this is altitude region of the ionospheric dynamo, where the ion cyclotron and ion-neutral collision frequencies are equal. At 12:00 UT, the maximum disagreement is 25% at 150 km, while at 00:00 UT, the maximum disagreement is a factor of four. The source of this discrepancy is related to how SIC and IRI handle nighttime ionization in the *E* region ionosphere, which is predominantly caused by emission sources such as Lyman- α and Lyman- β . It is not surprising that with low ionization rates (relative to direct, daytime ionization), even small differences in the estimated source ionization rates can lead to noticeable differences. Even during this worst case, the combined estimated error of the IRI and SIC ion and electron densities could account for such a difference. Future work may be warranted to further refine nighttime ionization estimates.

[19] With good agreement between the expected compilations in Figure 1 and the IRI-based model above 120 km, we have established a reasonable confidence in the SIC-based conductivity model. Additional comparisons with measurements at various altitudes would certainly be beneficial and should be attempted in the future. In this paper, we want to demonstrate one of the most useful advances of the SIC-based conductivity model, inclusion of energetic particle precipitation as an ionization source.

3. MINIS Balloon Campaign

[20] One of the MINIS Balloon payloads was aloft during the onset of the SEP event on 20 January 2005 and made in situ stratospheric conductivity measurements. These

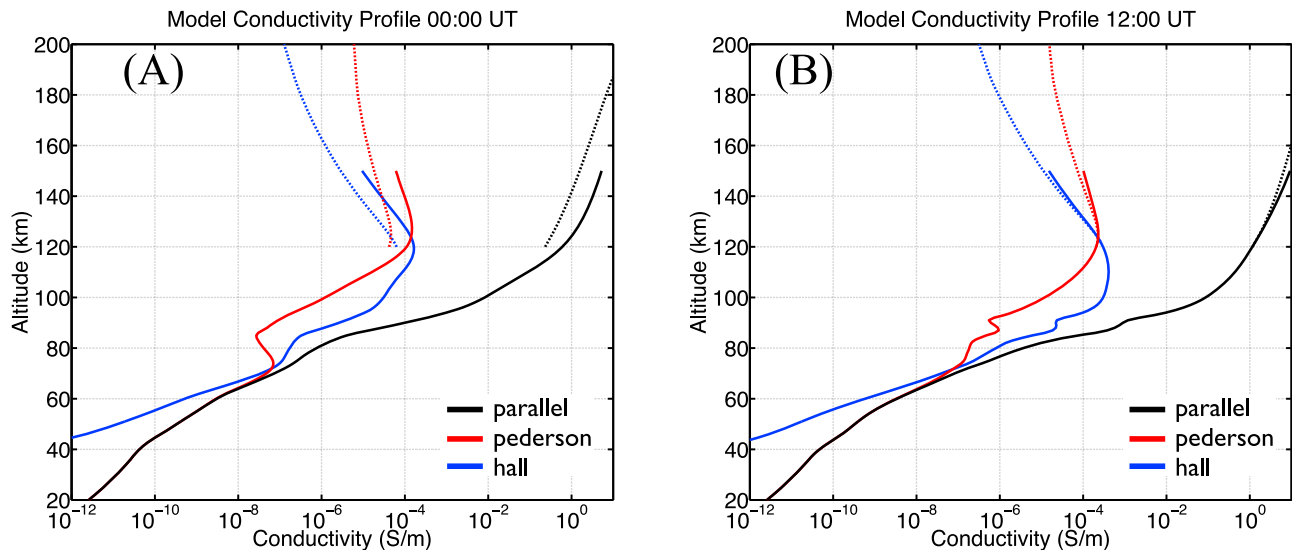


Figure 4. Modeled parallel (black), Pedersen (red) and Hall (blue) conductivity profiles for two separate times on 20 January 2005 at 345°E, 70°S geographic. Each conductivity component is calculated using IRI ion densities above 120 km (dashed) while the SIC ion densities are used below 150 km (solid), such that there are overlaps between 120 km and 150 km. No energetic particle precipitation is considered in any of these conductivity profile calculations. (a) The conductivity modeled at 00:00 UT (beginning of 20 January 2005), which is local sunset/sunrise and as close to nighttime as this latitude gets in summer. There is a maximum difference between the IRI and SIC-based conductivities of nearly a factor of 4. (b) Conductivity at 12:00 UT with maximum difference of 25% between the IRI and SIC-based conductivity.

measurements can be directly compared with the SIC-based conductivity model results.

3.1. MINIS Overview

[21] The primary objective of the MINIature Spectrometer (MINIS) campaign was to observe REP X-rays at multiple locations simultaneously in order to help resolve some of the temporal and spatial ambiguity of previously observed precipitation. The main phase of the MINIS balloon campaign consisted of two sets of balloon payload launches. One set was launched from the Southern Hemisphere site at the South African National Antarctic Expedition (SANAE) IV (71.7°S, 2.8°W geographic), while the other set launched from Fort Churchill, Manitoba, Canada (58.8°N, 265.9°E geographic). Each Southern Hemisphere payload included an X-ray spectrometer, dc electric field instrumentation, a magnetometer, GPS receiver and an Iridium satellite modem for telemetry. The Northern Hemisphere payloads were similar, but had no electric field probes. The Southern Hemisphere flights had battery life to last for ~8-day flights and the Northern Hemisphere payloads were designed to last for ~1–2 days. The data presented here are exclusively from one of the Southern Hemisphere payloads. All data were telemetered to a ground station at the Space Sciences Laboratory in Berkeley, California using the Iridium satellite communication network. A GPS receiver was used to measure geographic latitude, longitude and altitude. The entire payload was rotated about the vertical axis by a dc electric motor with a period of about 45 s per rotation. Payload power was provided by several lithium ion battery packs.

3.2. Conductivity Measurement Technique

[22] During each southern flight, the vector dc electric field was measured using three sets of orthogonal double-

langmuir probes. Each probe was covered in a colloidal carbon suspension, called Aquadag, to provide a uniform surface work function. Electrical conductivity measurements were made during the MINIS balloon campaign using the relaxation time technique. This method has been used many times for stratospheric balloon observations [e.g., *Bering et al.*, 2003; *Byrne et al.*, 1988; *Few and Weinheimer*, 1986; *Holzworth*, 1991]. The basic idea of this technique is to place charge onto one of the electric field probes, and then measure the time constant associated with the probe returning to equilibrium. The time constant for relaxation to ambient floating voltage depends inversely on the conductivity of the medium around the probe. A complete description of the technique theory is described by *Chang and Kodera* [1985]. In the case of the MINIS payloads, conductivity was measured during a calibration cycle every 10 min. After being biased +3.2 V or –3.2 V through a high-impedance relay, the probes returned to an equilibrium potential of the surrounding collisional plasma with a characteristic exponential time constant τ . This time constant is related to conductivity through the following relation:

$$\sigma = \frac{\epsilon_0}{\tau} \quad (11)$$

The probe potential was sampled 10 times per second during the calibration cycle such that relaxation times longer than 1/10th second can be resolved. Figure 5 shows an example of a relaxation curve from which a time constant and conductivity are calculated. When probes are biased with respect to the ambient plasma, in order to equilibrate, they must gather charge carriers of opposite polarity. Thus, conductivity observations made using this technique are polar (not total) measurements. The total conductivity is the sum

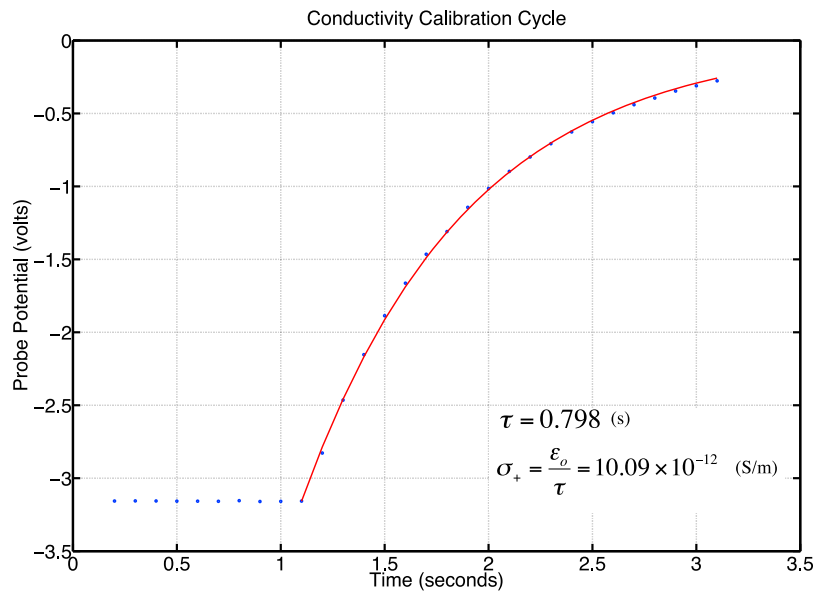


Figure 5. An example MINIS balloon conductivity measurement. The dots are data points showing a negative probe bias and positive ion collection. The red line shows an exponential fit to the data (R -square = 0.99) giving a 0.798-s decay time constant.

of the conductivity due to both positive and negative charge carriers.

$$\sigma = \sigma_+ + \sigma_- = \frac{\epsilon_o}{\tau_+} + \frac{\epsilon_o}{\tau_-} \quad (12)$$

In the stratosphere near the balloon float altitude of 32 km, there are very few free electrons and essentially all of the charge carriers are positive and negative ions. Since the average mass and number density of negative and positive ions are nearly equal in the stratosphere, roughly half of the conductivity is a result of each polarity charge carrier.

[23] Photoemission can affect conductivity measurements of positive charge carriers. A photoemission current combined with a current of positive ions will cause a probe to relax back into electrostatic equilibrium faster than the ions alone. This has the effect of decreasing the relaxation time constant, from which an artificially high positive atmospheric conductivity can be calculated. *Byrne et al.* [1990] determined that under normal circumstances, this photoemission can be as large as a factor of three for Aquadag-covered spherical probes. The negative conductivity is not subject to the same contamination because the probe is biased positively. When electrons are photo-emitted, they do not have enough energy to surpass the electrical force pulling them back to the probe. Thus, the emitted electrons return to the probe surface resulting in a zero net photocurrent. During the 20 January 2005 SEP event, daytime positive polarity conductivity measurements were up to three times higher than the negative polarity measurements (not shown). There is evidence that suggests the ozone concentration above the balloon dropped as a result of SEP precipitation [*Degenstein et al.*, 2005; *Seppälä et al.*, 2006]. A drop in ozone levels could result in higher UV flux reaching the balloon and therefore increased photo-ionization. In order to mitigate possible UV flux contamination of the total

conductivity measurement for this study, the negative polarity conductivity measurements were assumed to account for half of the total conductivity. Thus, the atmospheric conductivity values shown later in Figure 8 are twice the measured negative polarity values.

4. 20 January 2005 SEP Event Overview

[24] January 2005 was a particularly active period for the sun. During the declining phase of solar cycle 23, between 15 January and 24 January, there were five X-class solar flares observed by the GOES X-ray detectors. In conjunction with some of these solar flares, several halo coronal mass ejections (CMEs), and SEP events occurred. Solar flare X-rays, bulk CME plasma and energetic particles each affect the Earth's coupled magnetosphere-ionosphere-atmosphere system. In this case study, effects of the hardest SEP event, which occurred on 20 January 2005 are presented.

[25] Figure 6 shows GOES energetic protons from GOES 10 and 11 on 20 January 2005. In January 2005, GOES 10 was the west operational satellite at 135°W and GOES 11 was in a back-up position at 105°W. GOES 12 proton data were not available for this time period. Integral proton intensity is given in seven different channels (I1 > 1 MeV, I2 > 5 MeV, I3 > 10 MeV, I4 > 30 MeV, I5 > 50 MeV, I6 > 60 MeV and I7 > 100 MeV). Data from GOES 10 channels I6 and I7 were not available during this time period. The SEP event onset is marked with a vertical dashed line labeled SEP. Even before the onset time, proton intensity values are elevated because of the SEP events during several preceding days. A rapid increase in all energy channels occurs at the SEP-event onset. From GOES 11, the >100 MeV proton channel increases by four orders of magnitude in a matter of minutes. Recall that the SIC-based conductivity model assumes that all particles measured at geosynchronous precipitate into the polar caps. For comparison

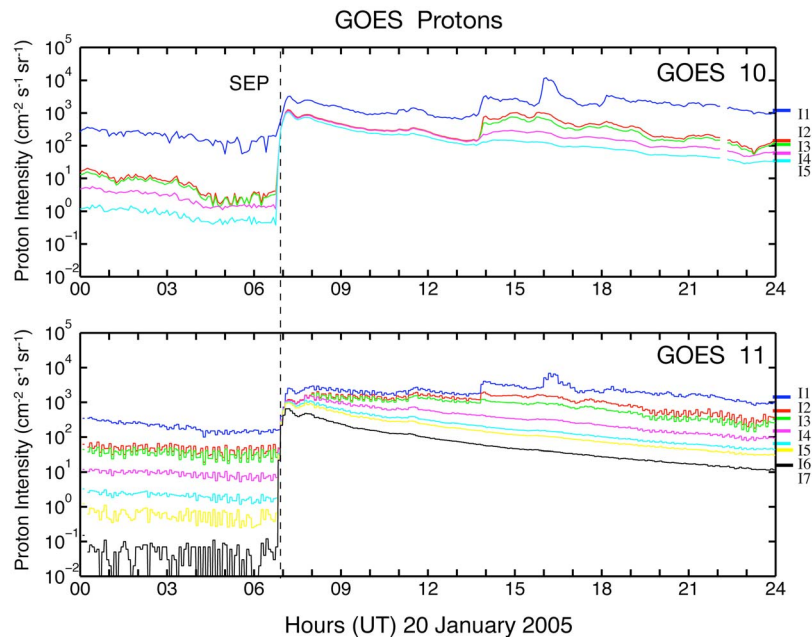


Figure 6. GOES 10 and 11 integral energetic proton intensity on 20 January 2005. The seven integral channels, I1 to I7, are shown in blue, red, green, magenta, cyan, yellow and black, respectively. The minimum proton energy for each channel: I1 > 1 MeV, I2 > 5 MeV, I3 > 10 MeV, I4 > 30 MeV, I5 > 50 MeV, I6 > 60 MeV and I7 > 100 MeV. The vertical dashed line represents the SEP event onset at GOES 10 and 11.

with stratospheric balloon-based conductivity measurements, low-energy flux is not important because only protons with energy near 100 MeV or more can penetrate down to the balloon altitude near 32 km. Only protons that reach the balloon altitude will cause local ionization resulting in a conductivity enhancement.

[26] The GOES observations provide an estimate of the proton flux precipitating into the polar cap. However, the MINIS balloon was not in the middle of the polar cap, but slightly closer to the equator in the sub-auroral zone. The Earth's geomagnetic field regulates the how far toward the equator a proton can precipitate in the form of rigidity cutoffs. Rigidity cutoffs can be estimated as geomagnetic latitudinal boundaries. Protons of a given energy precipitate nearly uniformly everywhere pole-ward of its specific cutoff latitude. Equator-ward of the cutoff, no protons below the same given energy precipitate. Rigidity cutoffs are not static and vary with geomagnetic activity [Smart *et al.*, 2003; Rodger *et al.*, 2006]. However, cutoff position and dynamics (on time scales of hours or less) are inherently difficult to measure or model for a specific case. Therefore, we use the Polar Operational Environment Satellites (POES) 15, 16, and 17 proton data to get a reasonable estimate of the proton cutoff modulating the precipitation above the MINIS balloon.

[27] Figure 7a shows a map containing the MINIS Flight 2 South ground track on 20 January 2005, following the SEP event onset as well as the magnetic field line footprint tracks for three nearby passes of POES 15, 16, and 17. Three sets of markers indicate the balloon location and a POES footprint location when one satellite passed nearby geographically

and was at nearly the same geomagnetic latitude indicated by IGRF L-contours. The specific locations, separations and L-values are given in Table 2. These pairs of locations represent the best estimates of the precipitating proton spectral measurements above the balloon during the SEP event. Figures 7b–7d show energetic proton integral intensity spectrograms for the three passes shown in Figure 7a. Each spectrogram is based on data from 16-s averaged POES MEPED P6, P7, P8 and P9 channels which correspond to minimum proton energy thresholds of 16 MeV, 35 MeV, 70 MeV, and 140 MeV, respectively [Evans and Greer, 2000 (rev. 2006)]. Linear interpolations to the logarithm (base 10) of the intensity are used to fill in the spectra between the threshold values at each time step. Solid black vertical lines in Figures 7b–7d indicate the time associated with each set of markers in Figure 7a. The pair of dashed black vertical lines indicates the edges of the map in Figure 7a. In Figure 7b, outside of the polar cap at 09:22:00 UT, the POES 17 > 140 MeV integral proton intensity is <10 ($\text{s}^{-1} \text{cm}^{-2} \text{sr}^{-1}$), while deep inside the polar cap, the intensity plateaus near 78 ($\text{s}^{-1} \text{cm}^{-2} \text{sr}^{-1}$) after 09:30:00 UT. POES 17 crosses the same L contour (4.17) as the balloon at 09:27:16 UT, when the >140 MeV proton intensity is 55.88 ($\text{s}^{-1} \text{cm}^{-2} \text{sr}^{-1}$), less than the polar cap plateau intensity. Therefore, at 09:27:16 UT, POES 17 was at a location where the proton cutoff was greater than 140 MeV and, by analogy, so was the balloon. Later, the balloon appears to be outside of the 140 MeV cutoff at 16:43:08 UT when POES 16 observed the near-balloon >140 MeV proton intensity at 13.77 ($\text{s}^{-1} \text{cm}^{-2} \text{sr}^{-1}$) when the polar cap values was plateaued near 17 ($\text{s}^{-1} \text{cm}^{-2} \text{sr}^{-1}$). The picture remains similar at 20:00:51 UT when POES 15

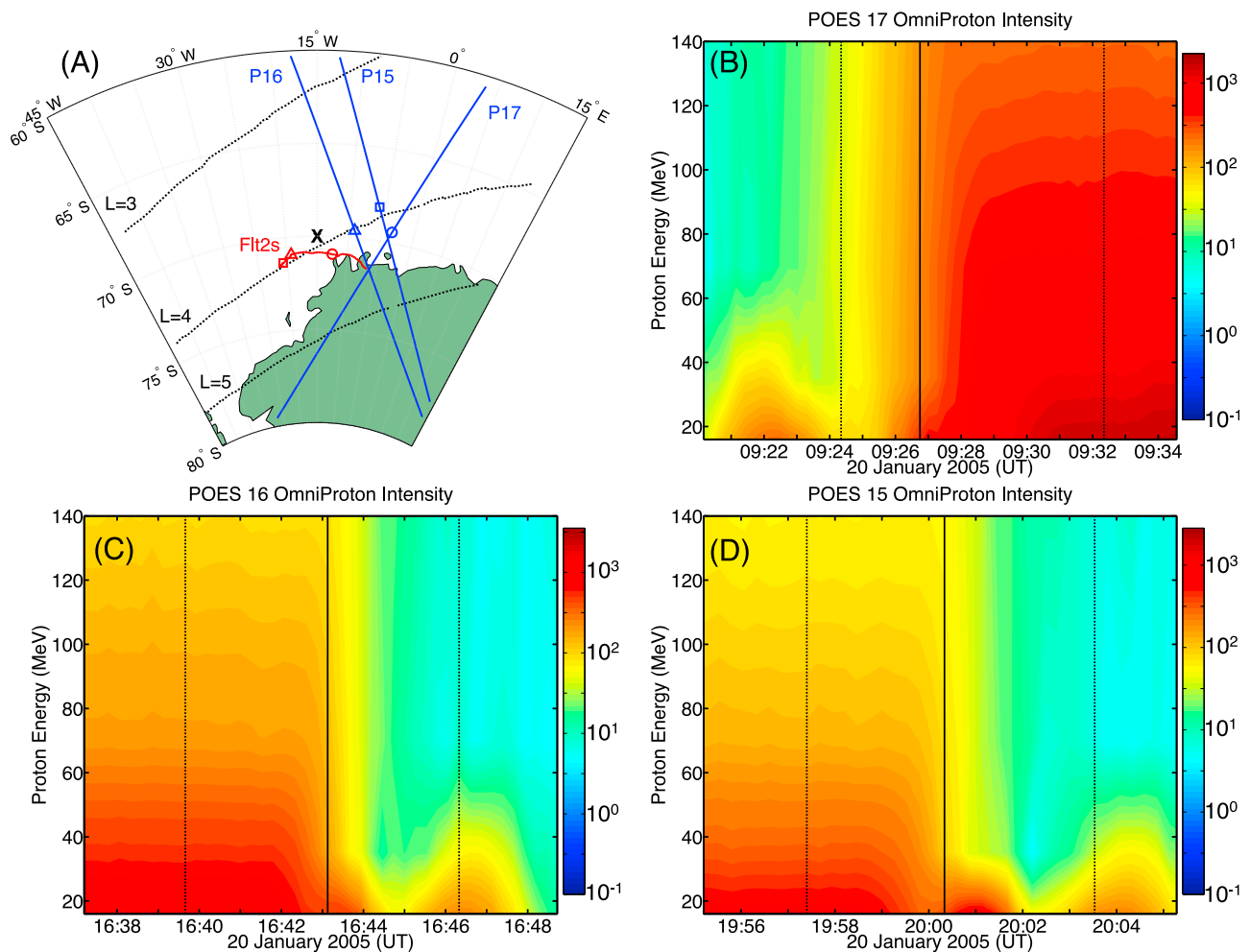


Figure 7. POES energetic proton observations in the vicinity of the MINIS Flight 2 South (Flt2s) balloon. (a) The ground track of Flt2s in red and three magnetic footprint tracks for three nearby POES satellite passes. The “X” at 70°S, 15°W indicates the representative location of the balloon over the course of the day used in the conductivity model. Dashed lines represent L contours and continental Antarctica is shaded green. Pairs of markers indicate specific locations where the balloon and a POES satellite were close in geographic coordinates and at nearly the same geomagnetic latitude. (b–d) The integral proton intensity (protons $s^{-1} cm^{-2} sr^{-1}$) measured using the POES MEPED. Solid black vertical lines correspond to the time of the marked locations. Dashed black vertical lines represent the times when the satellite track is at the edges of the map in Figure 7a. Figures 7b (POES 17), 7c (POES 16), and 7d (POES 15) correspond to circle, triangle, and square markers, respectively.

observed the near-balloon >140 MeV proton intensity at 4.47 ($s^{-1} cm^{-2} sr^{-1}$) when the polar cap values were plateaued near 9 ($s^{-1} cm^{-2} sr^{-1}$). It is clear from these comparisons that the balloon was near the 140 MeV cutoff location for duration of the SEP event. There were almost certainly some shifts in the precipitating proton spectrum due to rigidity cutoff motion (Kp

varied between 1 and 4 on 20 January 2005) and the motion of the balloon. With three nearby POES passes, it appears that the balloon was always at a location where the precipitating proton spectrum was cut off somewhere above 140 MeV. In the next section, where modeled and observed conductivity are compared, we select modeled cutoff values of 150 MeV and

Table 2. MINIS Balloon Flight 2 South and POES Locations Identified in Figure 7^a

Time (UT)	Symbol	POES	B-lat (°S)	B-lon (°W)	F-lat (°S)	F-lon (°W)	Distance (km)	L-value
09:27:16	Circle	17	70.94	12.51	69.14	3.44	381.70	4.17
16:43:08	Triangle	16	70.94	19.33	69.60	9.18	408.61	4.02
20:00:51	Square	15	71.35	20.76	68.18	5.89	649.74	3.91

^aEach row gives the time (UT), the symbols used in Figure 7 to identify the balloon and satellite magnetic field line footprint pair, the POES satellite identifier, balloon geographic latitude (B-lat), balloon geographic longitude (B-lon), satellite magnetic field line footprint latitude (F-lat), satellite magnetic field line footprint longitude (F-lon), the distance separating the balloon location and satellite footprint location, and the L-value of the satellite.

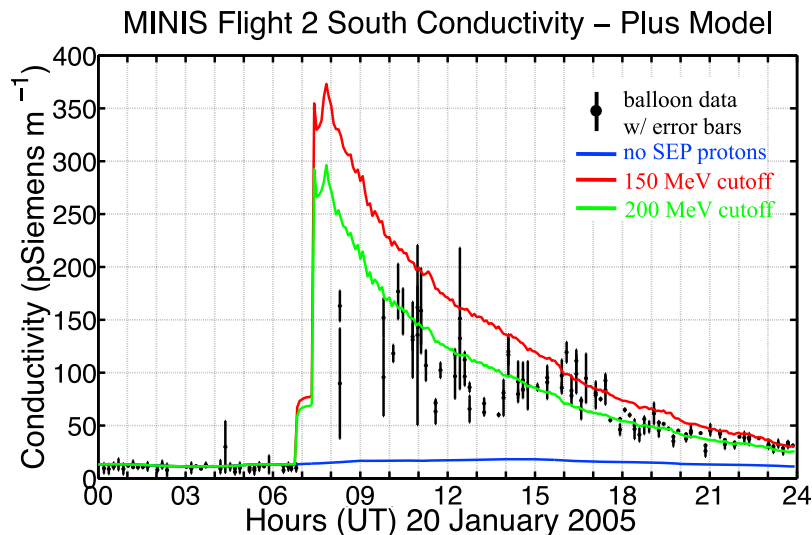


Figure 8. Conductivity observations from MINIS Flight 2 South and modeled conductivity. The observations with the associated error are in black. The upper (red) curve is a model result assuming a cutoff of 150 MeV protons. Similarly, the middle (green) curve assumes a 200 MeV proton cutoff. The bottom (blue) curve assumes no precipitating protons. Incident proton spectra are taken from GOES 11.

200 MeV as reasonable estimates for the physical cutoff at the balloon location.

5. Conductivity Model and Data Comparison

[28] Shortly after the SEP event onset on 20 January 2005, the local electrical conductivity at MINIS Balloon Flight 2 South was observed to increase by a factor of about 20. Figure 8 shows the measured conductivity for 20 January 2005. There are a few points to note about the conductivity measurements on this day. First, the frequency of the data points decreases dramatically after the SEP event onset. This is a result of how the onboard computer was programmed to accept data and place it into the telemetry stream. Counts from the X-ray scintillator were the highest priority data for the campaign and were placed into the data stream preferentially. When the count rate during the SEP event greatly exceeded the expected REP count rate for a sustained period of time, other data were lost, including conductivity data. The second point to note is that the 95% confidence error bars after the SEP event onset are larger. This is a result of sampling frequency. During conductivity calibration cycles, the voltages on the electric field probes were sampled ten times per second. The nominal relaxation time in the stratosphere near 30 km is about 1 s. However, with a 20-fold increase of conductivity, the goodness of fit statistics for the calculated exponential decay time constants worsened. Even though the conductivity data generally worsened in quality after the SEP event onset, we have confidence that the instrumentation was making valid measurements. In a properly functioning double Langmuir probe instrument on a balloon payload rotated about the vertical axis, a quasi-dc horizontal electric field appears as a sinusoid with the same frequency as the rotation. A discussion by *Kokorowski* [2008] shows that this signature sinusoidal oscillation is present throughout the SEP event, ensuring that a valid potential, which is the basis of both the conductivity and

electric field observations, is being measured. Despite these instrumental effects, the basic trend is clear, after the SEP event onset, there was a very large conductivity increase.

[29] In Figure 8, modeled conductivity is overlaid on the balloon measurements. The conductivity model input parameters included specifying the location of 70°S and 345°E, which is used as a representative of the balloon location during the SEP event. Two model conductivity curves are calculated corresponding to a cutoff of 150 MeV (red) and 200 MeV (green). The input spectrum used for making Figure 8 was taken from GOES 11. Rigidity cutoffs were taken into account by simply including only the portion of the integral intensity spectrum (e.g., the circles in Figure 3) above the desired cutoff energy. The large jump from 10 pS/m to over 250 pS/m is directly related to the SEP event onset and the dramatic increase in proton precipitation. The smaller discontinuities are results of re-estimating the differential GOES proton spectrum for each 5-min interval. Each set of GOES integral proton flux measurements were converted into a differential spectrum by assuming a spectral shape described in equation (8). This results in a variable ionization rate in the SIC model and variable conductivity.

[30] Before the SEP event onset, the modeled and observed conductivity are the same to within the estimated errors. After the SEP event onset, both SIC-based conductivity model curves agree fairly well with the MINIS Flight 2 South observations, especially after 09:00 UT. Without a more accurate estimate of the local, time-dependent rigidity cutoff at the balloon location, a more precise comparison between the model and measurements is not practical. Even so, the agreement with the balloon measurements before and during the SEP event is clearly evident. Looking back at Figure 1, between 30 km and 40 km, the 1969 SEP event caused a conductivity enhancement between zero and three orders of magnitude. When applying the SIC-based model to the 20 January 2005 event, the largest discrepancy is no more than a factor of two and often within the measurement

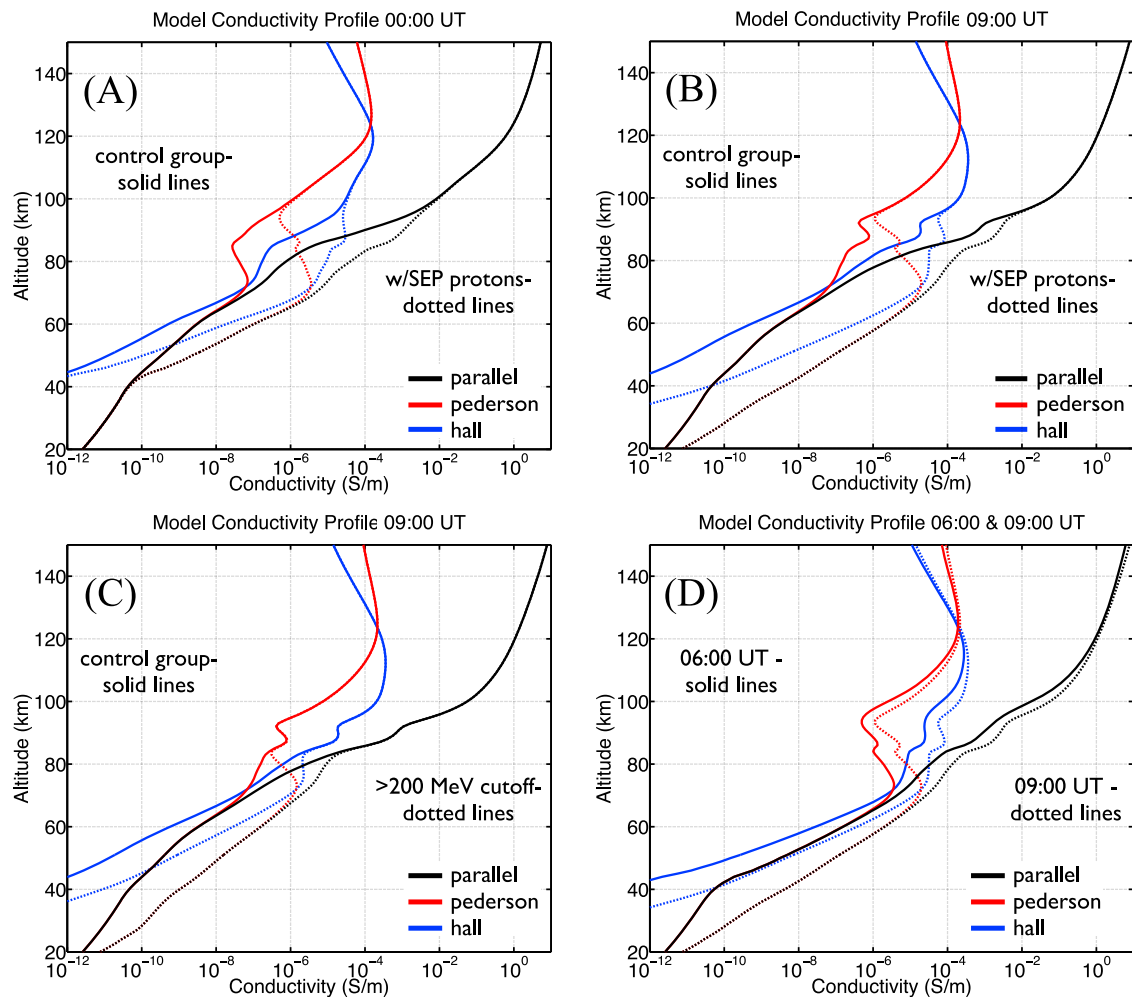


Figure 9. Comparisons of modeled conductivity under various conditions. Each panel contains two sets of conductivity profiles including parallel (black), Pedersen (red) and Hall (blue) terms. All of the results are for a specific location, 345°E , 70°S geographic on 20 January 2005. (a) Conductivity profiles of a “control” group (solid) with no included SEP proton precipitation and a “full” proton spectrum (dashed) are shown for 00:00 UT, before the hard SEP event onset at 06:51 UT. (b) The same “control” (solid) and “full” (dashed) conductivity profile sets for 09:00 UT, after the SEP event onset. (c) The same as Figure 9b except that a 200 MeV cut off was assumed. (d) Two profile sets that include the “full” SEP proton spectrum for 06:00 UT (before the SEP event onset; solid) and 09:00 UT (after the onset; dotted).

error estimates. From this model comparison with measurements, direct ionization of neutrals by incident precipitating SEP protons can account for most, if not all, of the conductivity increase observed by MINIS Flight 2 South.

[31] The MINIS conductivity enhancement observations are the only in situ balloon-borne stratospheric measurements during such a hard and prolonged SEP event. On 16 February 1984, *Holzworth et al.* [1985] measured a peak conductivity enhancement of a factor of ~ 2 from a balloon at -56.3° invariant latitude that lasted for less than two hours. The proton flux above 100 MeV was much weaker during the 16 February 1984 event when compared than the 20 January 2005 event (< 2 orders of magnitude increase at geostationary in 1984 compared to > 4 orders of magnitude increase in 2005). Additionally, the 1984 event was shorter in duration, with the geostationary > 100 MeV proton flux returning to pre-event levels in nearly 15 h. In 2005, 15 h

after the SEP event onset, the 100 MeV electron flux was still elevated by 2 orders of magnitude.

6. Conductivity Model Results for 20 January 2005 SEP Event

[32] We can estimate electrical conductivity at any altitude between 20 km and 150 km during 20 January 2005 using the SIC-based conductivity model. Examples of conductivity enhancements are shown for the entire day for the full altitude range of the model. In this section, we present the SIC-based conductivity model results during the course of the day, before and after the SEP event onset at 06:51 UT.

[33] Figure 9 shows several different conductivity profile comparisons. Figures 9a–9d shows two sets of conductivity profiles, each containing parallel (solid line), Pedersen (dashed) and Hall (lightly dashed) profiles. The purpose of each panel is to illustrate how the conductivity changed at

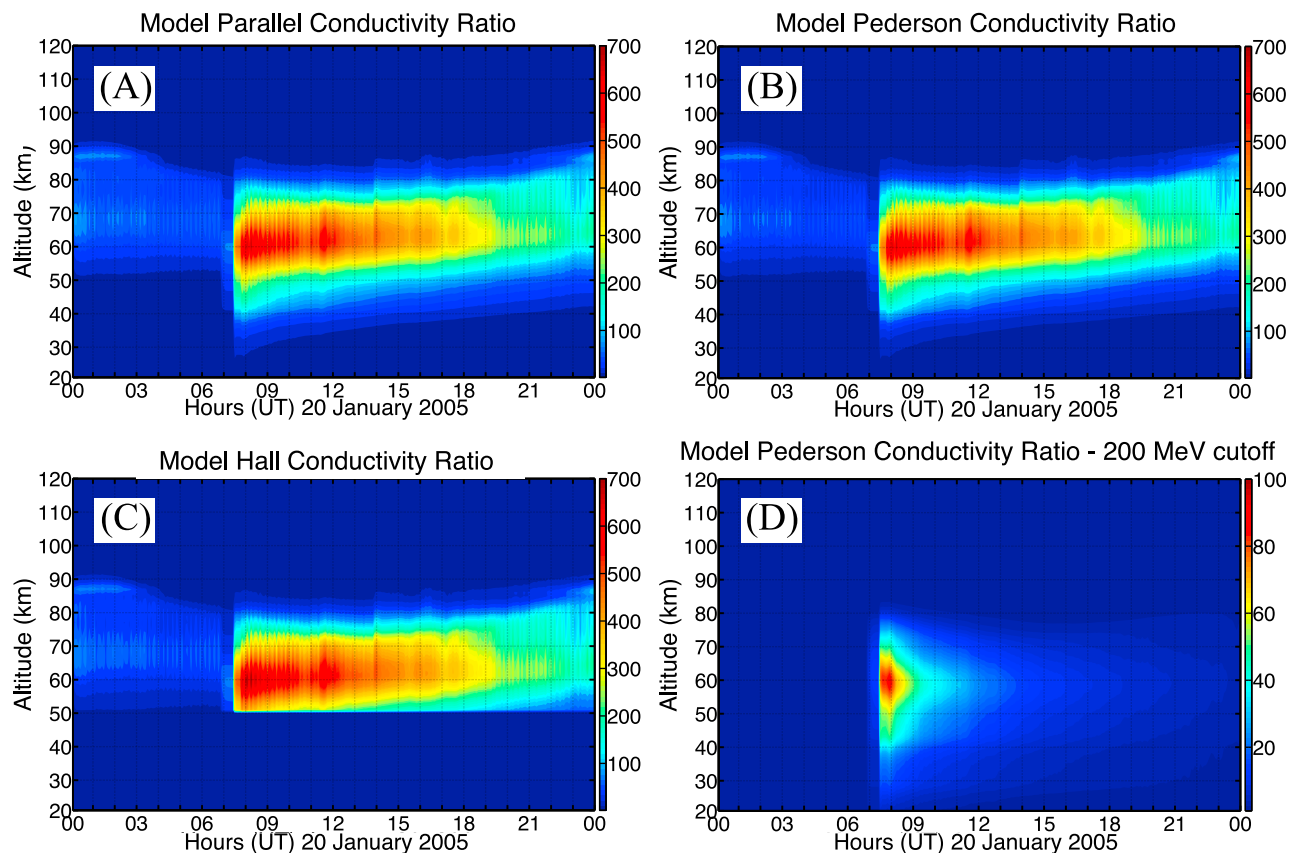


Figure 10. Complete conductivity enhancement spectra for the entirety of 20 January 2005, showing the relative enhancement of one component of SIC-based conductivity. Altitude in kilometers is indicated on the vertical axis, and time in hours UT on 20 January 2005 is shown on the horizontal axis. The color indicates the multiplicative enhancement of conductivity when SEP proton ionization is included with respect to modeled conductivity with no proton precipitation. For example, a color corresponding to 300 means that the conductivity component is 300 times greater when protons are included. The (a) parallel, (b) Pedersen and (c) Hall terms, with a full SEP proton spectrum. (d) Pedersen conductivity with a 200 MeV cutoff. The color bar in Figures 10a–10c ranges from 1 to 700, while Figure 10d has a maximum of 100. The lower altitude (below 50 km) region of the Hall term in Figure 10c is artificially set to unity because Hall conductivity does not have much meaning in this range.

each altitude under various conditions. All profiles in Figure 9 were calculated for the same location (70°S , 345°E geographic) at different times of day and assuming one of three possible incident overhead proton spectra: (1) “control,” or no proton flux; (2) a “full” SEP spectrum with no rigidity cutoff; or (3) a 200 MeV cutoff. Again, the proton flux was taken from GOES 11 measurements. Figure 9a shows a control group of profiles along with a set of profiles with a full SEP spectrum at 00:00 UT on 20 January 2005. With the full SEP spectrum, each conductivity component is enhanced relative to the control group between 40 km and 100 km. This enhancement is a result of precipitating protons from an earlier SEP event. There is no conductivity increase at 32 km, near the balloon altitude. The same conditions are shown in Figure 9b, but at 09:00 UT. Here, the enhancement due to the SEP proton precipitation is larger by more than two orders of magnitude at 60 km, with altered conductivity expected down to the lower 20 km altitude limit of the model. A low-altitude enhancement is consistent with an increase in energetic proton flux during

the initial hours of this extremely hard SEP event. Figure 9c is the same as Figure 9b except that the incident SEP spectrum is cutoff at 200 MeV. The enhancements are generally lower than the full SEP spectrum case and the affected altitude range decreases to below 90 km. Figure 9d is slightly different in that each profile assumes a full SEP spectrum at two different times: 06:00 UT, before the large SEP event onset and 09:00 UT, several hours after onset. This plot is meant to illustrate the difference in observed conductivity before and after SEP event onset including both nominal solar irradiance and the SEP-induced enhancement.

[34] Figure 10 shows much of the same data as in Figure 9, but for the entire day. Each panel shows the multiplicative conductivity enhancement between a control group with no SEP precipitation and a group assuming either the full SEP flux (Figures 10a–10c) or a 200 MeV cutoff (Figure 10d). The color in each plot represents a multiplicative enhancement over the control group model. For example, a yellow color representing 300 means that the modeled conductivity with SEP flux included was 300 times

greater than the conductivity assuming no SEP flux. The parallel, Pedersen and Hall conductivity enhancements are shown in Figures 10a–10c, respectively. Figure 10d shows the Pedersen conductivity with a 200 MeV cutoff. Notice that the maximum color bar value in Figures 10a–10c is 700; while in Figure 10d it is only 100. There is a noticeable 5-min “beating” in each panel, most prominent at higher altitudes. This is a result of the model’s 5-min temporal step size. At each step, GOES 11 integral flux was converted into a differential spectrum. Each spectrum had a slightly different fit and resulted in a slightly different assumed incident proton flux. Figure 10c shows the Hall conductivity enhancement with altitude range below 50 artificially set to unity. This was done because the idea of a Hall term does not have much meaning at these altitudes because the collisional conductivity completely dominates.

[35] Each case in Figure 10 shows several commonalities between model estimates. Every conductivity component has a maximum enhancement near 60 km, regardless of the rigidity cutoff assumed. Also, there is essentially no enhancement above 95 km. This is well below the ionospheric dynamo altitude predicted to be between 110 km and 130 km. This implies that magnetospheric currents that close in the polar ionosphere would be essentially unchanged by this SEP event. The bulk of the ionization is simply too low. However, this version of the SIC-based conductivity model includes only protons and does not contain effects from any other particles that may be precipitating (i.e., alphas, heavier ions, or electrons). Daily solar ultraviolet is included in the model as described earlier, but photons specifically from the solar flare, which accompanied the SEP event, are not included. It is possible that the cumulative effects from these excluded particles may have a noticeable effect on D and E region ionospheric conductivity, but more effort is needed to investigate these interactions in detail. However, our initial estimates indicate minimal relative ionization in the E region resulting from protons. Consequently, inclusion of additional particles is saved for future analyses. Vertical atmospheric currents, which move from the ionosphere all the way to the ground through the maximum conductivity enhancements, might be affected on a global scale. Investigations on the effect of an SEP event on global atmospheric electrodynamics could include similar SIC-based conductivity model results.

7. Conclusion

[36] In this paper, we present evidence for direct SEP-induced ionization as the only physical mechanism needed to account for a rapid, dramatic 20-fold increase in observed sub-auroral stratospheric conductivity. The 20 January 2005 SEP event was the hardest event measured since 1956 and therefore had a large proton population above 100 MeV, which ionized the neutral atmosphere at and below the balloon altitude near 32 km.

[37] This study utilized several standard modeling tools as well as the relatively new SIC model to estimate the electrical conductivity between 20 and 150 km before and during the 20 January 2005 SEP event. POES energetic proton observations suggest that the balloon observation was near the 140 MeV proton cutoff during the SEP event. By including cutoff effects in the conductivity estimates, we

found a good agreement between data and model estimates. This agreement provides strong evidence that the precipitating protons are, indeed, the primary ionization source. Without including other external sources, SEP proton-induced ionization is estimated to have led to a more than 600-fold increase in the conductivity near 60 km. Relatively small conductivity enhancements (two- to fivefold) are thought to have occurred above 70 km as a result of SEP ionization, while almost no enhancement is thought to have occurred above 95 km. This study focused only on solar protons and did not consider any additional direct ionization in the atmosphere–ionosphere from solar photons (X-ray and UV) or other precipitating particles (electrons, alphas, heavier ions). It is possible that these sources could have increased the conductivity even more than simply by protons alone. Although the total effect of these additional sources is not addressed here, we suspect that solar photons would have a shorter temporal effect because the flare X-ray enhancements do not last as long as proton enhancements (several hours as opposed to more than a day) and any other precipitating particles would have a smaller overall effect because of relatively lower flux values. Further work is needed to fully evaluate the effects of additional ionization sources.

[38] The SIC-based conductivity model also shows the utility of the Sodankylä Ion and Neutral Chemistry Model. Without this tool, estimates for the charged particle carried densities would not have been as robust. By combining standard tools and the SIC model, we have developed a globally applicable conductivity model that can be used at any location under a large variety of conditions, notably energetic particle precipitation.

[39] **Acknowledgments.** Portions of this work were funded by the National Science Foundation under grant numbers: ANT-0230441, ATM-0408356, and ATM-0649489. Other portions were carried out at the Jet Propulsion Laboratory, California Institute of Technology, under a contract with the National Aeronautics and Space Administration.

[40] Robert Lysak thanks the reviewers for their assistance in evaluating this paper.

References

- Bailey, D. K. (1964), Polar-Cap Absorption, *Planet. Space Sci.*, 12(5), 495–541, doi:10.1016/0032-0633(64)90040-6.
- Bering, E. A., et al. (2003), Long term changes in the electrical conductivity of the stratosphere, *Adv. Space Res.*, 32, 1725–1735, doi:10.1016/S0273-1177(03)90469-8.
- Bethe, A. H., and J. Ashkin (1953), Passage of Radiations through Matter, in *Experimental Nuclear Physics*, vol. 1, edited by E. Segre, pp. 166–251, John Wiley & Sons, New York.
- Bilitza, D. (1990), International Reference Ionosphere 1990, *Rep. NSSDC 90-22*, Natl. Space Sci. Data Cent./World Data Cent. A for Rockets and Satell., Greenbelt, Md. [Available at <http://iri.gsfc.nasa.gov/>.]
- Byrne, G. J., et al. (1988), Observations of the Stratospheric Conductivity and Its Variation at 3 Latitudes, *J. Geophys. Res.*, 93(D4), 3879–3891, doi:10.1029/JD093iD04p03879.
- Byrne, G. J., et al. (1990), Solar-Radiation (190–230 Nm) In The Stratosphere - Implications For Photoelectric Emissions From Instrumentation At Balloon Altitudes, *J. Geophys. Res.*, 95(D5), 5557–5566, doi:10.1029/JD095iD05p05557.
- Chang, J. S., and K. Kodera (1985), Theory of electric-conductivity measurements by an electrostatic-probe in an atmospheric low-density continuum ionized-gas, *J. Geophys. Res.*, 90(D4), 5897–5900, doi:10.1029/JD090iD04p05897.
- Ciliverd, M. A., et al. (2005), Modeling a large solar proton event in the southern polar atmosphere, *J. Geophys. Res.*, 110, A09307, doi:10.1029/2004JA010922.
- Ciliverd, M. A., et al. (2006), Ionospheric evidence of thermosphere-to-stratosphere descent of polar NO_x, *Geophys. Res. Lett.*, 33, L19811, doi:10.1029/2006GL026727.

- Clilverd, M. A., et al. (2007), Improved dynamic geomagnetic cutoff modeling: Testing predictive accuracy, *J. Geophys. Res.*, *112*, A08302, doi:10.1029/2007JA012410.
- Degenstein, D. A., et al. (2005), Observations of mesospheric ozone depletion during the October 28, 2003 solar proton event by OSIRIS, *Geophys. Res. Lett.*, *32*, L03S11, doi:10.1029/2004GL021521.
- Evans, D. S., and M. S. Greer (2000), Polar orbiting environmental satellite space environment monitor –2: Instrument descriptions and archive data documentation, *NOAA Tech. Memo. OAR SEC-93, Rev. 2.0*, Space Environ. Cent., Boulder, Colo.
- Few, A. A., and A. J. Weinheimer (1986), Factor of 2 error in balloon-borne atmospheric conduction current measurements, *J. Geophys. Res.*, *91*(D10), 937–948.
- Freier, P. S., and W. R. Webber (1963), Exponential rigidity spectrums for solar-flare cosmic rays, *J. Geophys. Res.*, *68*(6), 1605–1629, doi:10.1029/JZ068i006p01605.
- Friedrich, M., and K. M. Torkar (2001), FIRI: A semiempirical model of the lower ionosphere, *J. Geophys. Res.*, *106*(A10), 21,409–21,418, doi:10.1029/2001JA900070.
- Hale, L. C. (1984), Middle atmosphere electrical structure, dynamics and coupling, *Adv. Space Res.*, *4*(4), 175–186, doi:10.1016/0273-1177(84)90283-7.
- Heaps, M. G. (1978), Parameterization of cosmic-ray ion-pair production-rate above 18 km, *Planet. Space Sci.*, *26*(6), 513–517, doi:10.1016/0032-0633(78)90041-7.
- Hedin, A. E. (1991), Extension of the MSIS thermosphere model into the middle and lower atmosphere, *J. Geophys. Res.*, *96*(A2), 1159–1172, doi:10.1029/90JA02125.
- Holzworth, R. H. (1991), Conductivity and electric field variations with altitude in the stratosphere, *J. Geophys. Res.*, *96*(D7), 12,857–12,864, doi:10.1029/91JD00119.
- Holzworth, R. H. (1995), Quasistatic electromagnetic phenomena in the atmosphere and ionosphere, in *Handbook of Atmospheric Electrodynamics*, edited by H. Volland, pp. 235–266, CRC Press, Boca Raton, Fla.
- Holzworth, R. H., M. C. Kelley, C. L. Siefring, L. C. Hale, and J. D. Mitchell (1985), Electrical measurements in the atmosphere and the ionosphere over an active thunderstorm. 2. Direct current electric fields and conductivity, *J. Geophys. Res.*, *90*(A10), 9824–9830, doi:10.1029/JA090iA10p09824.
- Holzworth, R. H., K. W. Norville, and P. R. Williamson (1987), Solar flare perturbations in stratospheric current systems, *Geophys. Res. Lett.*, *14*(8), 852–855, doi:10.1029/GL014i008p00852.
- Jackman, C. H., M. T. DeLand, G. J. Labow, E. L. Fleming, D. K. Weisenstein, M. K. W. Ko, M. Sinnhuber, J. Anderson, and J. M. Russell (2005a), The influence of the several very large solar proton events in years 2000–2003 on the neutral middle atmosphere, *Adv. Space Res.*, *35*(3), 445–450, doi:10.1016/j.asr.2004.09.006.
- Jackman, C. H., M. T. DeLand, G. J. Labow, E. L. Fleming, D. K. Weisenstein, M. K. W. Ko, M. Sinnhuber, and J. M. Russell (2005b), Neutral atmospheric influences of the solar proton events in October–November 2003, *J. Geophys. Res.*, *110*, A09S27, doi:10.1029/2004JA010888.
- Jones, J. B. L., et al. (2005), Space weather and commercial airlines, *Adv. Space Res.*, *36*(12), 2258–2267, doi:10.1016/j.asr.2004.04.017.
- Kirkwood, S., et al. (1988), Ionospheric conductivities, electric-fields and currents associated with auroral substorms measured by the Eiscat radar, *Planet. Space Sci.*, *36*(12), 1359–1380, doi:10.1016/0032-0633(88)90005-0.
- Kokorowski, M. (2008), Energetic particle precipitation effects on the electrodynamics of the coupled magnetosphere-ionosphere-atmosphere, PhD thesis, Dep. of Earth and Space Sci., Univ. of Washington, Seattle.
- Kokorowski, M., et al. (2006), Rapid fluctuations of stratospheric electric field following a solar energetic particle event, *Geophys. Res. Lett.*, *33*, L20105, doi:10.1029/2006GL027718.
- Lowes, F. J. (2010), The international geomagnetic reference field: A “health” warning, <http://www.ngdc.noaa.gov/IAGA/vmod/igrfw.html>, Natl. Geophys. Data Cent., Boulder, Colo.
- Maus, S., et al. (2005), The 10th generation international geomagnetic reference field, *Phys. Earth Planet. Inter.*, *151*(3–4), 320–322, doi:10.1016/j.pepi.2005.03.006.
- Mewaldt, R. A., M. D. Looper, C. M. S. Cohen, G. M. Mason, D. K. Haggerty, M. I. Desai, A. W. Labrador, R. A. Leske, and J. E. Mazur (2005), Solar-particle energy spectra during the large events of October–November 2003 and January 2005, in *Proceedings of the 29th International Cosmic Ray Conference, August 3–10, 2005, Pune, India*, vol. 1, pp. 111–114, Tata Inst. of Fundam. Res., Mumbai, India.
- Parks, G. K. (1991), *Physics of Space Plasmas*, Westview, Boulder, Colo.
- Picone, J. M., et al. (2002), NRLMSISE-00 empirical model of the atmosphere: Statistical comparisons and scientific issues, *J. Geophys. Res.*, *107*(A12), 1468, doi:10.1029/2002JA009430.
- Rees, M. H. (1989), *Physics and Chemistry of the Upper Atmosphere*, Cambridge Univ. Press, Cambridge, U. K.
- Reid, G. C. (1961), Study of enhanced ionization produced by solar protons during a polar cap absorption event, *J. Geophys. Res.*, *66*(12), 4071–4085, doi:10.1029/JZ066i012p04071.
- Reid, G. C. (1986), Electrical structure of the middle atmosphere, in *The Earth's Electrical Environment*, edited by the Natl. Res. Council et al., pp. 183–194, Natl. Acad. Press, Washington, D. C.
- Rodger, C. J., et al. (2006), Dynamic geomagnetic rigidity cutoff variations during a solar proton event, *J. Geophys. Res.*, *111*, A04222, doi:10.1029/2005JA011395.
- Rodger, C. J., et al. (2007), Lightning-driven inner radiation belt energy deposition into the atmosphere: Implications for ionisation-levels and neutral chemistry, *Ann. Geophys.*, *25*(8), 1745–1757, doi:10.5194/angeo-25-1745-2007.
- Seppälä, A., et al. (2004), Solar proton events of October–November 2003: Ozone depletion in the Northern Hemisphere polar winter as seen by GOMOS/Envisat, *Geophys. Res. Lett.*, *31*, L19107, doi:10.1029/2004GL021042.
- Seppälä, A., et al. (2006), Destruction of the tertiary ozone maximum during a solar proton event, *Geophys. Res. Lett.*, *33*, L07804, doi:10.1029/2005GL025571.
- Seppälä, A., et al. (2008), The effects of hard-spectra solar proton events on the middle atmosphere, *J. Geophys. Res.*, *113*, A11311, doi:10.1029/2008JA013517.
- Smart, D. F., et al. (2003), Evaluation of the dynamic cutoff rigidity model using dosimetry data from the STS-28 flight, in *Space Weather 2000*, edited by T. G. Onsager et al., pp. 841–846, Oxford, New York, doi:10.1016/S0273-1177(02)00800-1.
- Tinsley, B. A., and L. Zhou (2006), Initial results of a global circuit model with variable stratospheric and tropospheric aerosols, *J. Geophys. Res.*, *111*, D16205, doi:10.1029/2005JD006988.
- Tobiska, W. K., et al. (2000), The SOLAR2000 empirical solar irradiance model and forecast tool, *J. Atmos. Sol. Terr. Phys.*, *62*(14), 1233–1250, doi:10.1016/S1364-6826(00)00070-5.
- Turunen, E., et al. (1996), *D-region ion chemistry model*, in *STEP Handbook of Ionospheric Models*, edited by R. W. Schunk, pp. 1–25, SCO-STEP Secretariat, Boulder, Colo.
- Verronen, P. T. (2006), Ionosphere–atmosphere interaction during solar proton events, PhD thesis, Dep. of Phys. Sci., Univ. of Helsinki, Helsinki.
- Verronen, P. T., et al. (2002), Modelling the effects of the October 1989 solar proton event on mesospheric odd nitrogen using a detailed ion and neutral chemistry model, *Ann. Geophys.*, *20*(12), 1967–1976, doi:10.5194/angeo-20-1967-2002.
- Verronen, P. T., et al. (2005), Diurnal variation of ozone depletion during the October–November 2003 solar proton events, *J. Geophys. Res.*, *110*, A09S32, doi:10.1029/2004JA010932.